Memristive Devices with Highly Repeatable Analog States Boosted by Graphene Quantum Dots

*Changhong Wang, Wei He, Yi Tong, Yishu Zhang, Kejie Huang, Li Song, Shuai Zhong, Rajasekaran Ganeshkumar, and Rong Zhao**

Memristive devices, having a huge potential as artificial synapses for low-power neural networks, have received tremendous attention recently. Despite great achievements in demonstration of plasticity and learning functions, little progress has been made in the repeatable analog resistance states of memristive devices, which is, however, crucial for achieving controllable synaptic behavior. The controllable behavior of synapse is highly desired in building neural networks as it helps reduce training epochs and diminish error probability. Fundamentally, the poor repeatability of analog resistance states is closely associated with the random formation of conductive filaments, which consists of oxygen vacancies. In this work, graphene quantum dots (GQDs) are introduced into memristive devices. By virtue of the abundant oxygen anions released from GQDs, the GQDs can serve as nano oxygen-reservoirs and enhance the localization of filament formation. As a result, analog resistance states with highly tight distribution are achieved with nearly 85% reduction in variations. In addition the insertion of GQDs can alter the energy band alignment and boost the tunneling current, which leads to significant reduction in both switching voltages and their distribution variations. This work may pave the way for achieving artificial neural networks with accurate and efficient learning capability.

1. Introduction

The world of "big data" has dramatically evolved in the recent years, from explosive data growth to the way in which data are structured and used. This generates enormous challenges in data storage, processing, and analysis. Compared with conventional computation relying on the von Neumann architecture, brain-inspired computing has shown superior strength in various cognitive tasks, such as image processing and speech recognition.[1–3] It has been widely accepted that information in the brain is represented by vastly interconnected synapses and formed by modification of synapses and neural networks.[4,5] The emulation of synapse is crucial for developing brain-like computing systems (i.e., artificial neural networks). As a promising candidate for artificial synapses, memristive devices (i.e., memristors) have sparked a new wave of research enthusiasm, and significant accomplishments in the plasticity and learning functions of synapses have been reported in recent years.[6–14] To achieve high-density artificial neural networks, analog resistance states of memristive devices are preferred in mimicking the adjustable synaptic weights, which sets stringent requirements on analog switching. It has been reported that the poor repeatable analog resistance states of memristive devices require a high number of training epochs, which would result in low-efficient operation and energy waste.[15,16] Moreover, it may increase the programming error probability of neural networks.[2,3] Hence, it is crucial for memristive devices to possess high repeatable analog resistance states; however, little progress has been made until now.

C. Wang, Dr. W. He, Dr. Y. Tong, Y. Zhang, Dr. K. Huang, L. Song, S. Zhong, R. Ganeshkumar, Prof. R. Zhao
Engineering Product Development
Singapore University of Technology and Design (SUTD)
8 Somapah Road, 487372, Singapore
E-mail: zhao_rong@sutd.edu.sg

DOI: 10.1002/smll.201603435

ADVANCED SCIENCE NEWS
www.advancedsciencenews.com

On the other side, graphene quantum dots (GQDs) are edge-functionalized nanometer dimension graphene fragments.[17–20] Bonding with functional groups, GQDs possess fascinating optical and electronic properties because of quantum confinement and edge effects. The unique optoelectronic properties and ample material availability make GQDs fascinating for diverse applications, spanning from energy to life sciences.[19–22] But the unique characteristic of the abundant and easily detached oxygen functional groups of GQDs has not been exploited, which may enable novel applications beyond the existing techniques.

In this work, we introduce GQDs into memristive devices. The insertion of GQD can alter the energy band alignment and boost the tunneling current of the device. More importantly, the GQDs bond with abundant and easily detached oxygen functional groups. By virtue of the atomic-level oxygen functional groups (especially, oxygen anions) released from GQDs, the stochastic nature of oxygen vacancy formation and migration, which deteriorates the repeatability of analog resistance states, can be minimized for valence change mechanism based memristive devices. As a result, compared with control samples, memristive devices with GQDs demonstrate highly repeatable analog resistance states with nearly 85% reduction in variations. Besides, switching voltages are reduced by 40% and their distributions are also narrowed by 84%. This work not only expands the applications of GQDs to new area, but also paves the way for attaining controllable artificial synapses, which may equip neural networks with accurate and efficient learning capability.

2. Results and Discussion

2.1. Graphene Quantum Dots and Their Thermal Stability

GQDs (purchased from ACS Materials company) were synthesized by hydrothermal methods. A transmission electron microscopy (TEM) image (**Figure 1**a) shows that the GQDs are monodisperse and have a mean diameter of 4.3 nm (Figure 1d). A high-resolution TEM image of a representative GQD (Figure 1b) shows the poor crystallinity of GQDs. The corresponding fast Fourier transformation scattering pattern (Figure 1c) reveals that GQDs have multilayer graphene fragments, which is consistent with previous reports.[23–27] The photoluminescence spectrum (Figure 1e) of the GQDs in isopropyl alcohol solution shows a broad peak at 526 nm excited by ultraviolet light of 365 nm, which is associated with the electronic structure and surface states of the GQDs.[28–30] The Fourier transform infrared spectrum (FT-IR) of GQDs (Figure 1f) indicates that there are oxygen functional groups in GQDs, such as hydroxyl (−OH), carboxyl (−COOH), carbonyl

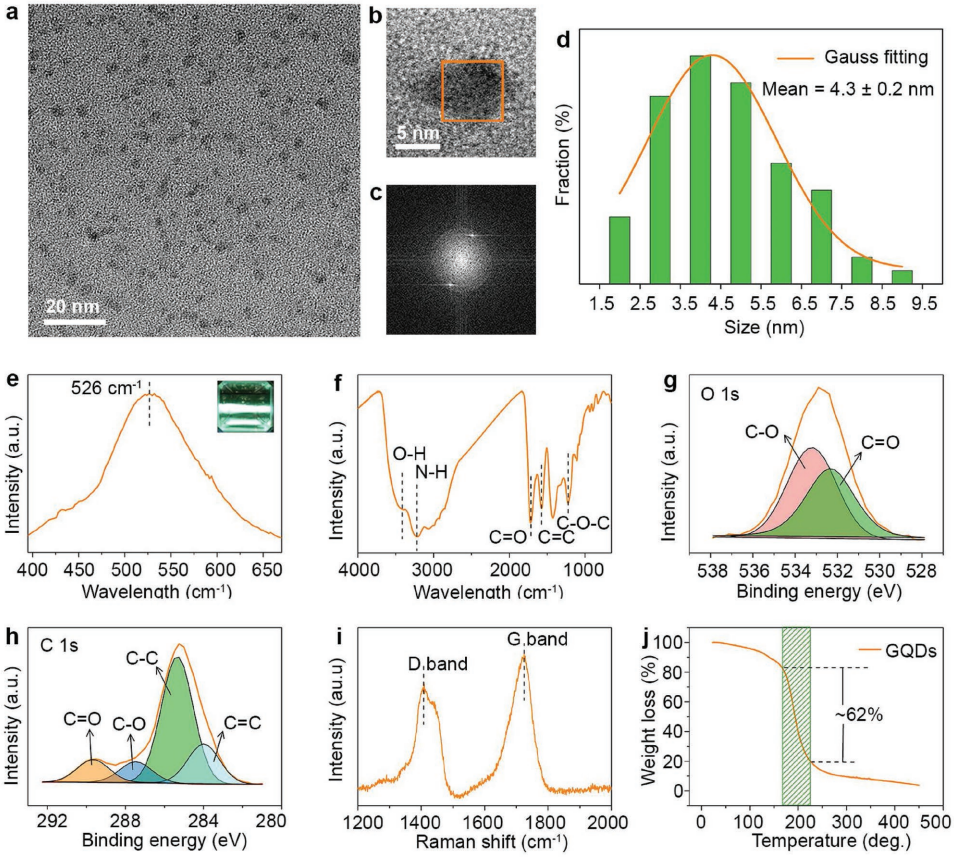

Figure 1. Characterizations of GQDs. a) TEM image of GQDs. b) High resolution TEM image of a GQD. c) Fast Fourier transformation (FFT) pattern of the single GQD. d) Size distribution. e) Photoluminescence spectrum excited at 365 nm. Inset is an onsite photoluminescence image. f) FT-IR spectrum. g) High-resolution O 1s spectra. h) High-resolution C 1s spectra. i) Raman spectrum. j) TGA profile.

(C=O), and epoxide (−O−). X-ray photoelectron spectroscopy was further performed to investigate these oxygen functional groups. There are two strong peaks observed at 284.8 and 532.2 eV (Figure S1, Supporting Information), corresponding to C 1s and O 1s signals, respectively. High-resolution O 1s spectra (Figure 1g) show that oxygen in GQDs mainly exists in C−O and C=O. High-resolution C 1s spectra (Figure 1h) illustrate that GQDs mainly contain C=C, C−C, C−O, and C=O, which are observed at 284.0, 285.3, 287.5, and 289.8 eV, respectively. Moreover, the intensity of C−C is much stronger than that of C=C, indicating the existence of abundant oxygen functional groups in GQDs. This fact was further verified by Raman spectrum (Figure 1i). It shows a disordered (D) band at 1405 cm^{-1} and a crystalline (G) band at 1719 cm^{-1}. The intensity ratio of the D to the G band (I_D/I_G) is 0.92, meaning that there are massive structural defects in GQDs. This further verifies the stability of these oxygen functional groups in GQDs. Thermal gravity analysis (TGA) was performed to investigate the thermal stability of GQDs. TGA profile (Figure 1j) shows that about 62% mass loss occurs at 175–225 °C, illustrating that the oxygen functional groups are easily detached at the elevated temperature. Based on above analysis, it can be concluded that the GQDs contain abundant oxygen functional groups, such as hydroxyl (−OH), carboxyl (−COOH), and epoxide (−O−), as depicted in the schematic diagram (**Figure 2**a), which are readily detached from the graphene framework. In addition, the ultrasmall sizes of GQDs and rich functional groups result in the poor crystallinity of GQDs (Figure 1b), which is in agreement with the reports.[17,18,21] In this work, the GQDs are introduced into memristive devices for potential performance boosting.

Memristive devices with GQDs (hereinafter, referred to as GQDMem) were fabricated through standard semiconductor processes as specified in the Experimental Section. The GQDs were embedded between the active layer (FeO_x) and the top electrode (Pt). In order to investigate the effect of GQDs in memristive devices clearly, memristive devices without GQDs (hereinafter, referred to as control memristors) were also fabricated for comparison.

2.2. Repeatability of Analog Resistance States

The memory performance of GQDMem was investigated under a direct current (DC) voltage sweeping mode. An electroforming process with 1 mA compliance current was performed to initialize resistive switching. The forming voltage of GQDMem is about 2.05 V (Figure 2b), which is much smaller than that of control memristor (≈3.5 V). Besides, the tunneling current of GQDMem is higher than that of control memristors before the abrupt switching. Both phenomena should be due to the integration of the GQDs into devices. **Figure 3**a shows a comparison of set/reset profiles between GQDMem and control memristors. The set and reset voltages of GQDMem are –0.7 and 1.0 V, respectively, which are smaller than those of control memristors (–1.5 and 1.5 V). Both voltages are reduced by about 40%. Besides, the maximum reset current in GQDMem decreases from 5 to 2 mA. The reductions in operation voltages and maximum reset current indicate that the introduction of GQDs into memristive devices can reduce power consumption. The repeatability of set/reset profiles for 50 consecutive cycles of GQDMem and control memristors is presented in Figure 3b,c, respectively. In contrast to the widespread distribution of set voltage (V_{set}) of control memristors, the *I–V* curves of 50 cycles of GQDMem nearly completely overlap with each other. The distribution of V_{set} and reset voltage (V_{reset}) for both devices is analyzed in cumulative probability plot (Figure 3d). Compared with control memristors, the coefficient of variation (CV) of V_{set} and V_{reset} of GQDMem decreases around 85% (from 9.9% to 1.6% and from 11.1% to 1.8% for V_{set} and V_{reset}, respectively), where the CV is defined as the ratio of the standard deviation (σ) to the mean value (μ). The histogram plots of distributions of V_{set} and V_{reset} for GQDMem and control memristors are depicted in Figure S2c,f (Supporting Information). It is worth noting that the voltage distributions of GQDMem outperform the previous reports.[31–35] Moreover, the distributions of memristive resistances are also greatly improved. A cumulative probability plot of the high resistance state (HRS) and the low resistance state (LRS) for GQDMem and control memristors is illustrated in Figure 3e. All the resistances in this work were read at 0.2 V bias. The

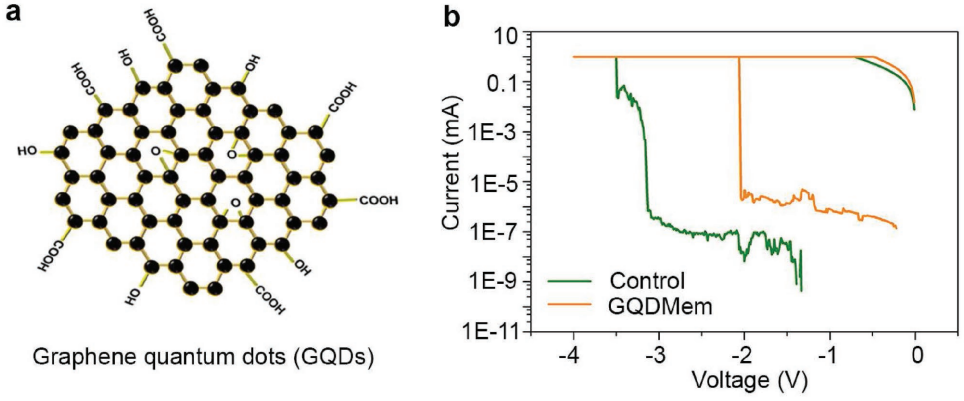

Figure 2. Electroforming process and analysis. a) Schematic diagram of GQD with oxygen functional groups. b) Electroforming processes of GQDMem and control memristors.

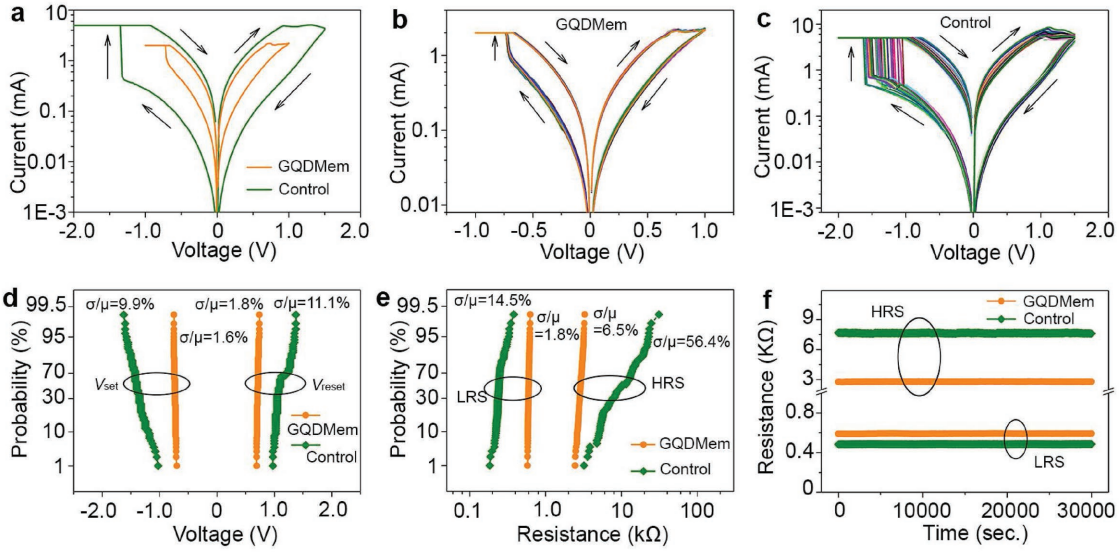

Figure 3. Discrete resistance states of GQDMem and control memristors in DC mode. a) Comparison of set/reset profiles between GQDMem and control memristors. b) DC voltage sweeping of GQDMem for 50 consecutive cycles. c) DC voltage sweeping of control memristors for 50 consecutive cycles. d) Distribution of the set/reset voltages of GQDMem and control memristors for 100 cycles. e) Distribution of HRS and LRS of GQDMem and control memristors for 100 cycles. f) Data retention of GQDMem and control memristors. All the data were read at 0.2 V.

CVs of resistances at HRS and LRS for GQDMem are significantly reduced by nearly 90% (from 56.5% to 6.50% and from 14.5% to 1.8%, respectively). Notably, the CVs of resistances for HRS and LRS also surpass the previous publications.[36–38] The data retentions of GQDMem and control memristors (Figure 3f) both demonstrate good non-volatility in the programmed states. Based on the above analysis between GQDMem and control memristors, it is clear that the introduction of GQDs can significantly improve the repeatability of resistive switching. Also, the device-to-device variations are also improved by introducing GQDs into memristive devices, as shown in Figure S3 (Supporting Information). In addition, it is worth noting that the ON/OFF ratio of GQDMem is dependent on the compliance current and reset voltage.[9,39,40] The comparison of On/OFF ratio between GQDMem and control memristors will be further analyzed in Figure 5.

2.3. Repeatable Analog States

In neural networks, memristive devices are promising candidate in serving as artificial synapses due to the simple structure and ion dynamic similarity. The spike-timing-dependent plasticity (STDP), which is recognized as one of the fundamental learning rules, has been widely emulated based on memristive devices.[8,41,42] The STDP was also demonstrated on FeO_x-based memristors (same as the control device in this work) in our previous reports.[41] In order to achieve the multiple scale of synaptic weights, a memristive device with analog resistance switching behaviors is preferred. Furthermore, to equip neural networks with accurate and efficient learning capability, as aforementioned, memristive devices are preferred to demonstrate repeatable analog resistance states with tight distribution.[43] Here, analog resistive switching behavior was deliberately analyzed. As shown in **Figure 4**a, GQDMem shows superb cycle-to-cycle consistency in overall *I–V* curves for 100 continuous cycles, even during the switching region, indicating the outstanding repeatability of analog resistance states. By contrast, the *I–V* curves of control memristors show large fluctuation (Figure 4b), revealing the poor repeatability of resistance states. The comparison of analog states at different voltages between GQDMem and control memristors is presented in Figure 4c, showing that the variation of analog resistance states of GQDMem is much smaller than that of control memristors.

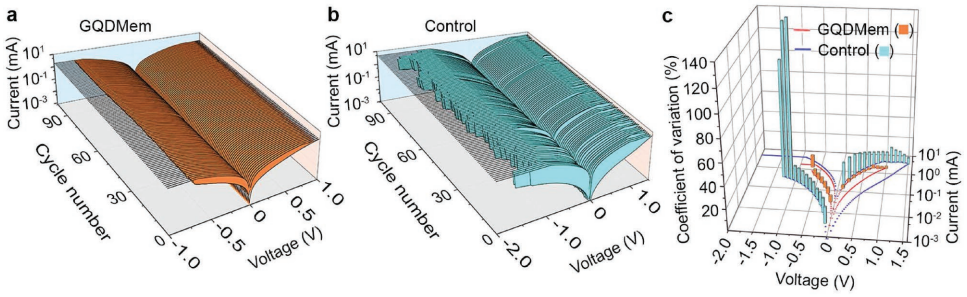

Figure 4. Comparison of repeatable analog resistance states of GQDMem and control memristors. a) *I–V* curves of GQDMem for 100 cycles. b) *I–V* curves of control memristors for 100 cycles. c) Comparison of variation of analog resistance states between GQDMem and control memristors.

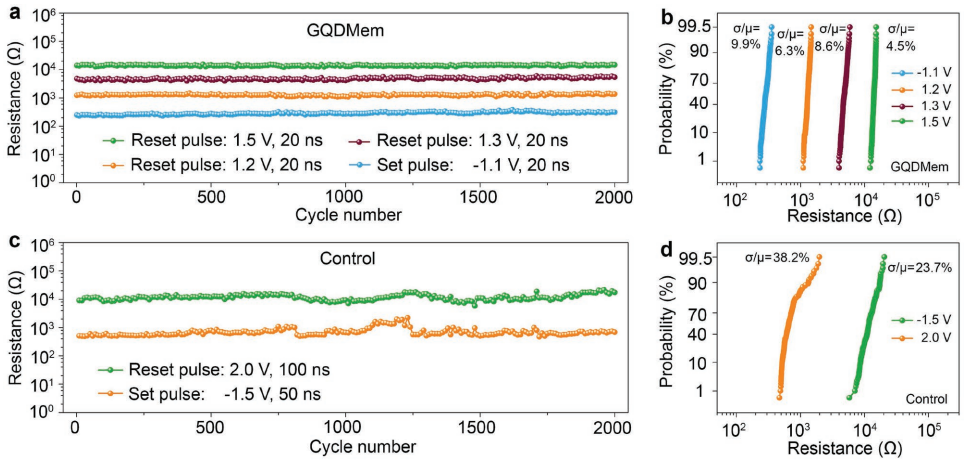

Figure 5. Characteristics of GQDMem and control memristors in pulse mode. a) Endurance of GQDMem with various voltage amplitudes, the resistances were read every 10 pulses. b) Distribution of multilevel resistances in GQDMem. c) Endurance of control memristors, the resistances were read every 10 pulses. d) Distribution of HRS and LRS in control memristors. All the data were read at 0.2 V.

Specifically, during the set process, the current variations at –0.25 V and –0.5 V (nonswitching region) in GQDMem are suppressed by 61% and 63%, respectively, compared with those of control memristors (Figure S4a,b, Supporting Information). More importantly, the current variation within the whole switching region of the set process is significantly reduced by as much as ≈89% (Figure S4c, Supporting Information). Similarly, during the reset process, the current variations at nonswitching region (0.25 and 0.5 V) and the whole switching region are dramatically reduced by 91%, 93%, and ≈88%, respectively (Figure S4d–f, Supporting Information). The analysis demonstrates that analog resistance states of GQDMem are highly repeated.

The memristive devices were further investigated under the pulse mode, which is the typical operation in circuits. By varying the pulse amplitude, the threshold voltages of set operation and reset operation, as illustrated in Figure S6 (Supporting Information), are found to be –0.95 V and 1.1, respectively. GQDMem and control memristors were cycled for 2000 consecutive pulses (**Figure 5**a,c). Compared with control memristors, the multilevel analog resistances of GQDMem are extremely stable during the endurance test without any obvious fluctuation. Besides, GQDMem exhibits an ON/OFF resistance ratio of about 50 times at a pulse of 1.5 V and 20 ns. In comparison, control memristors show a smaller ON/OFF ratio of about 15 times under a more powerful pulse (2.0 V, 100 ns). This indicates that the GQDMem improves the programming efficiency. The cumulative probabilities of the resistances of GQDMem and control memristors are replotted in Figure 5b,d, respectively. In contrast to control memristors, CVs of multilevel analog resistances of GQDMem are significantly improved by about 83% (from 38.2% to 6.3% and from 23.7% to 4.5% at 1 and 10 kΩ, respectively). In addition, the big tail at the right side of the low resistance curve of control memristors, which is unfavorable for circuit implementation, is greatly suppressed in GQDMem.[44] In brief, repeatable analog resistance states of GQDMem are demonstrated with tight distribution and without overlapping between any two resistance states.

For the application of artificial neural networks, synaptic plasticity of artificial synapses was investigated on GQDMem. Under a training protocol of 30 negative pulses (–1.6 V, 100 ns) followed by 30 positive pulses (1.6 V, 100 ns), GQDMem shows continuous increase (or decrease) in conductance as shown in Figure S5a (Supporting Information), which can be used to emulate the potentiation (or depression) of synapses in neuromorphic systems. Furthermore, the STDP can also be easily realized on GQDMem by modulating the pulse amplitude and width, as shown in Figure S5b (Supporting Information). These results indicate that GQDMem can serve as a good candidate of artificial synapses with improved repeatability.

2.4. Possible Microscopic Mechanism of Device Operation

Based on the experimental results, the significant improvement of GQDMem is definitely induced by the introduction of the GQDs. There are two possible reasons that may be related to the improvement of microscopic switching of GQDMem. First, because of abundant functional groups, GQDs exhibit an energy band gap, which will influence the band diagram of memristive devices (**Figure 6**a,b). When an external bias is applied to GQDMem, the energy band of oxides will be bended as shown in Figure 6b. The embedded GQDs may lower the conduction band offset for electrons and facilitate the tunneling at the low electric field, which results in the lower forming voltage and set/reset voltages. Another possible reason may correlate to the weak bond of oxygen functional groups (especially, oxygen anions). When the external bias increases, the temperature of the switching layer will increase due to the Joule heating.[45–48] When the elevated temperature exceeds 200 °C, oxygen-based atomic-level oxygen functional groups (especially, oxygen anions) start to detach from the GQD framework because of the weak chemical bond with the graphene fragment, as discussed in Figure 1. The detached atomic-level oxygen anions will easily drift into the switching material (here, iron oxide) along the direction of the electric field, serving as trapping

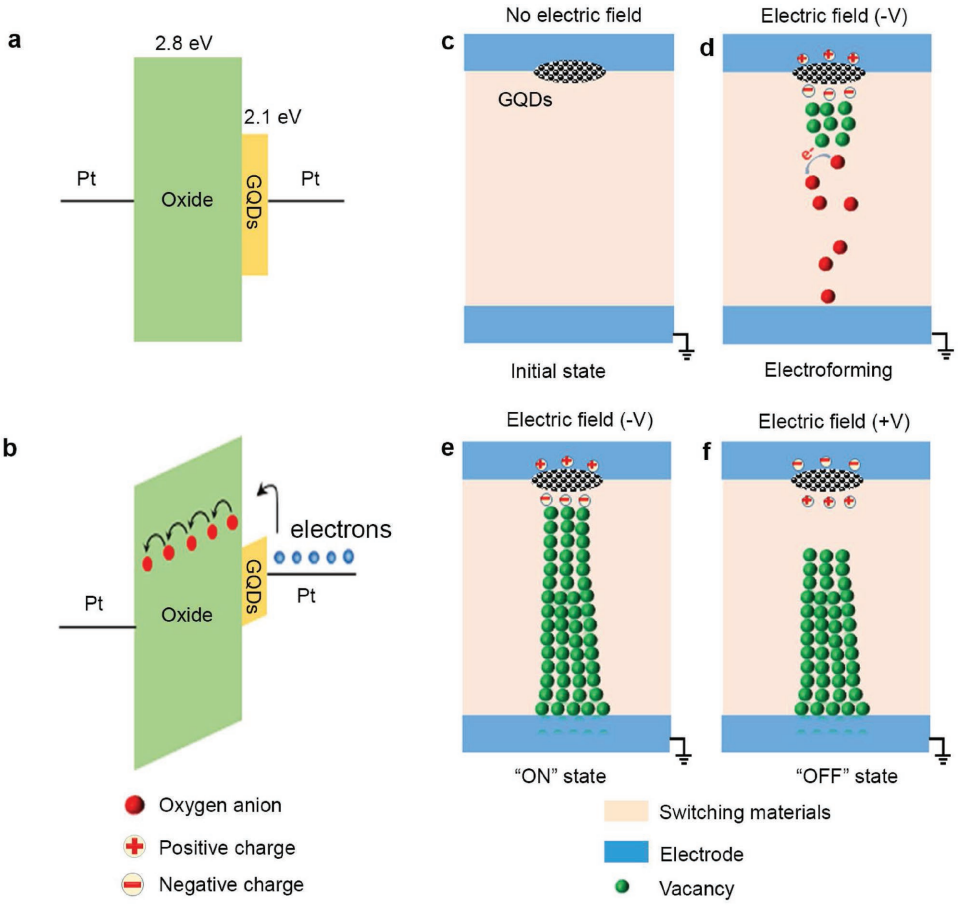

Figure 6. Microscopic switching mechanism of GQDMem. a) Flat band energy diagram of GQDMem. Representative bandgaps of FeO_x and GQDs are 2.8 and 2.1 eV, respectively. b) Energy band diagram of GQDMem under a bias. c) Pristine device. d) Electroforming process. Oxygen anions (red dots) released from GQDs facilitate the growth of CF, which is formed by oxygen vacancies (green dots). e) Set process. CF connects the bottom and top electrodes. f) Reset process. CF is ruptured around GQDs.

centers. The trapping centers will boost the tunneling current effectively and intensify Joule heating around them. It has been reported that the localized temperature can be higher than ≈700 °C due to the Joule heating during the operation.[48–50] Such high temperature can cause the bonds of metal oxide unstable. It is widely acknowledged that the resistive switching of memristive devices is closely associated with oxygen vacancies, which are generated from the break of metal–oxygen bonds under the combined effects of Joule heating and electric field.[10,45,46] The intensified heating would facilitate the metal–oxygen bond cleavage in FeO_x around trapping centers and generate a large amount of oxygen vacancies along the trapping centers, resulting in the localized formation of conductive filaments. The facilitation effect could be proved by the reduction of programming voltages.

In addtion because the energy band gap has less influence on the localized random nature, the big improvements in uniformity of programming voltages and resistance states indicates the detached oxygen functional groups (especially oxygen anions, −O−) is probably the dominant mechanism during the programming operations. To clearly illustrate the effects of GQDs on analog resistive switching, the microscopic mechanism was schematically shown in Figure 6. For a pristine memristive device, the GQDs with abundant oxygen functional groups reside at the top interface between the switching layer and the upper electrode (Figure 6c). The detached oxygen anions will drift into the switching layer along the electric field toward the bottom electrode, serving as trapping centers and facilitating the tunneling (Figure 6d). Most of the current would flow through the trapping centers and induce enhanced localized heat. As a result, the formation of conductive filaments (CF) is facilitated, which leads to the reduced electroforming voltage. Based on above analysis, the GQDs can be viewed as a nano oxygen-reservoir, providing abundant highly diffused oxygen anions. The nano oxygen-reservoir is able to seed and localize the growth of CF.

Similar to the electroforming process, with the assistance of the nano oxygen-reservoir, CF can be easily formed at low voltage during the set process (Figure 6e). During the reset process, GQDMem also shows great improvements in distributions of resistance and voltage as well as lower reset current. These improvements must be associated with the introduction of the nano oxygen-reservoir. The possible reason may relate to the quantum effect or the realignment of dipoles in GQDs under the reversed electric field, leading to the rupture of CF around GQDs (Figure 6f). However, the

exact role of the nano oxygen-reservoir in the reset process requires further investigation.

3. Conclusion

In this work, we introduce GQDs into memristive devices, serving as nano oxygen-reservoirs. The formation and migration of oxygen vacancies are manipulated by utilizing the oxygen anions released from GQDs. As a result, repeatable analog resistance states have been attained with nearly 85% reduction in variations, indicating highly controllable synaptic weight changes. Besides, switching voltages decrease by 40% and their distributions are narrowed by 84%. In addition, a resistive switching model is proposed to explain the possible underlying mechanism. This work indicates that GQDMem can serve as artificial synapses with controllable synaptic weight changes, equipping neural networks with accurate and efficient learning capability in terms of less training epochs and reduced programming error probability. Moreover, this approach could also be applied generally to other memristive devices with different materials and structures, boosting the further developments of artificial synapses for brain-inspired computing systems.

4. Experimental Section

Fabrication: Silicon wafers with 1 μm SiO_2 were used as the substrates. A 10 nm thick metallic titanium (Ti) serving as an adhesion layer was deposited on the substrates by radio frequency (RF) magnetic sputtering, then a 100 nm thick platinum (Pt) was deposited by e-beam evaporation as the bottom electrode. Subsequently, an 80 nm thick SiO_2 layer serving as an insulating layer was also deposited by e-beam evaporation. The active area with a diameter of 1 μm is formed. The 60 nm FeO_x switching layer was deposited by RF magnetic sputtering. To fabricate memristive devices with GQDs, the solutions of GQDs in isopropyle alcohol with the concentration of 1 mg mL^{-1} were used to coat on the top of FeO_x thin film by spin coating technique. Lastly, top electrode consisting of 100 nm Pt and 10 nm Ti was deposited by e-beam evaporation.

TEM Characterization: To observe the size of GQDs, the solution of GQDs was dropped on the copper grids and dried under infrared lamp. TEM analysis was conducted with the assistance of technicians in Win-Tech Nanotechnology Services Pte. Ltd..

Electrical Measurement: All the electrical characteristics were measured by a four-probe system (Cascade S300) equipped with a semiconductor characterization system (Keithley 4200-SCS). The various pulse conditions were engineered by Keithley 4200. During the electrical measurements, the bottom electrode was grounded. All measurements were performed at room temperature in air.

Supporting Information

Supporting Information is available from the Wiley Online Library or from the author.

Acknowledgements

This work was supported by Ministry of Education, Singapore (Grant No. 2013-T2-2-164), Singapore University of Technology and Design – Massachusetts Institute of Technology International Design Centre (Grant No. IDG31400103), and Singapore University of Technology and Design – Zhejiang University (Grant No. SUTD-ZJU/RES/05/2013). Meanwhile, the authors thank Dr. Xinyu Zhao for the characterization of photoluminescence.

[1] D. B. Strukov, G. S. Snider, D. R. Stewart, R. S. Williams, *Nature* **2008**, *453*, 80.
[2] Y. LeCun, Y. Bengio, G. Hinton, *Nature* **2015**, *521*, 436.
[3] V. Mnih, K. Kavukcuoglu, D. Silver, A. A. Rusu, J. Veness, M. G. Bellemare, A. Graves, M. Riedmiller, A. K. Fidjeland, G. Ostrovski, S. Petersen, C. Beattie, A. Sadik, I. Antonoglou, H. King, D. Kumaran, D. Wierstra, S. Legg, D. Hassabis, *Nature* **2015**, *518*, 529.
[4] T. Ohno, T. Hasegawa, T. Tsuruoka, K. Terabe, J. K. Gimzewski, M. Aono, *Nat. Mater.* **2011**, *10*, 591.
[5] S. Saïghi, C. G. Mayr, T. Serrano-Gotarredona, H. Schmidt, G. Lecerf, J. Tomas, J. Grollier, S. Boyn, A. F. Vincent, D. Querlioz, S. La Barbera, F. Alibart, D. Bichler, O. Vuillaume, C. Gamrat, B. Linares-Barranco, *Front. Neurosci.* **2015**, *9*, 51.
[6] M. Prezioso, F. Merrikh-Bayat, B. D. Hoskins, G. C. Adam, K. K. Likharev, D. B. Strukov, *Nature* **2015**, *521*, 61.
[7] L. Q. Zhu, C. J. Wan, L. Q. Guo, Y. Shi, Q. Wan, *Nat. Commun.* **2014**, *5*, 3158.
[8] S. H. Jo, T. Chang, I. Ebong, B. B. Bhadviya, P. Mazumder, W. Lu, *Nano Lett.* **2010**, *10*, 1297.
[9] C. Wang, W. He, Y. Tong, R. Zhao, *Sci. Rep.* **2016**, *6*, 22970.
[10] A. Wedig, M. Luebben, D.-Y. Cho, M. Moors, K. Skaja, V. Rana, T. Hasegawa, K. K. Adepalli, B. Yildiz, R. Waser, I. Valov, *Nat. Nanotechnol.* **2016**, *11*, 67.
[11] M. Wang, C. Bi, L. Li, S. Long, Q. Liu, H. Lv, N. Lu, P. Sun, M. Liu, *Nat. Commun.* **2014**, *5*, 4598.
[12] S. Balatti, S. Larentis, D. Gilmer, D. Ielmini, *Adv. Mater.* **2013**, *25*, 1474.
[13] J. Borghetti, G. S. Snider, P. J. Kuekes, J. J. Yang, D. R. Stewart, R. S. Williams, *Nature* **2010**, *464*, 873.
[14] J. Ali, G.-u.-d. Siddiqui, Y. J. Yang, K. T. Lee, K. Um, K. H. Choi, *RSC Adv.* **2016**, *6*, 5068.
[15] S. B. Eryilmaz, D. Kuzum, R. Jeyasingh, S. Kim, M. BrightSky, C. Lam, H.-S. P. Wong, *Front. Neurosci.* **2014**, *8*, 205.
[16] S. Yu, B. Gao, Z. Fang, H. Yu, J. Kang, H.-S. P. Wong, *Adv. Mater.* **2013**, *25*, 1774.
[17] K. A. Ritter, J. W. Lyding, *Nat. Mater.* **2009**, *8*, 235.
[18] L. Wang, Y. Wang, T. Xu, H. Liao, C. Yao, Y. Liu, Z. Li, Z. Chen, D. Pan, L. Sun, M. Wu, *Nat. Commun.* **2014**, *5*, 5357.
[19] L. Li, G. Wu, G. Yang, J. Peng, J. Zhao, J.-J. Zhu, *Nanoscale* **2013**, *5*, 4015.
[20] Z. Zhang, J. Zhang, N. Chen, L. Qu, *Energy Environ. Sci.* **2012**, *5*, 8869.
[21] Y. Li, Y. Zhao, H. Cheng, Y. Hu, G. Shi, L. Dai, L. Qu, *J. Am. Chem. Soc.* **2012**, *134*, 15.
[22] Y. Li, Y. Hu, Y. Zhao, G. Shi, L. Deng, Y. Hou, L. Qu, *Adv. Mater.* **2011**, *23*, 776.
[23] R. Ye, C. Xiang, J. Lin, Z. Peng, K. Huang, Z. Yan, N. P. Cook, E. L. G. Samuel, C.-C. Hwang, G. Ruan, G. Ceriotti, A.-R. O. Raji, A. A. Martí, J. M. Tour, *Nat. Commun.* **2013**, *4*, 2943.
[24] N. Suzuki, Y. Wang, P. Elvati, Z.-B. Qu, K. Kim, S. Jiang, E. Baumeister, J. Lee, B. Yeom, J. H. Bahng, J. Lee, A. Violi, N. A. Kotov, *ACS Nano* **2016**, *10*, 1744.

[25] T. S. Sreeprasad, A. A. Rodriguez, J. Colston, A. Graham, E. Shishkin, V. Pallem, V. Berry, *Nano Lett.* **2013**, *13*, 1757.
[26] G.-H. Kim, F. P. García de Arquer, Y. J. Yoon, X. Lan, M. Liu, O. Voznyy, Z. Yang, F. Fan, A. H. Ip, P. Kanjanaboos, S. Hoogland, J. Y. Kim, E. H. Sargent, *Nano Lett.* **2015**, *15*, 7691.
[27] G. Haider, P. Roy, C.-W. Chiang, W.-C. Tan, Y.-R. Liou, H.-T. Chang, C.- T. Liang, W.-H. Shih, Y.-F. Chen, *Adv. Funct. Mater.* **2016**, *26*, 620.
[28] X. Li, Y. Liu, X. Song, H. Wang, H. Gu, H. Zeng, *Angew. Chem. Int. Ed.* **2015**, *54*, 1759.
[29] X. Li, S. Zhang, S. A. Kulinich, Y. Liu, H. Zeng, *Sci. Rep.* **2014**, *4*, 4976.
[30] X. Li, M. Rui, J. Song, Z. Shen, H. Zeng, *Adv. Funct. Mater.* **2015**, *25*, 4929.
[31] S. Muraoka, K. Osano, Y. Kanzawa, S. Mitani, S. Fujii, K. Katayama, Y. Katoh, Z. Wei, T. Mikawa, K. Arita, Y. Kawashima, R. Azuma, K. Kawai, K. Shimakawa, A. Odagawa, T. Takagi, *Tech. Dig. Int. Electron Devices Meet.*, IEEE, Washington, DC, USA, **2007**, pp. 779–782.
[32] S. X. Wu, L. Z. Ren, F. M. Yu, K. G. Yang, M. Yang, Y. J. Wang, M. Meng, W. Q. Zhou, S. W. Li, *Appl. Phys. A: Mater. Sci. Process* **2014**, *116*, 1741.
[33] L.-W. Feng, C.-Y. Chang, Y.-F. Chang, T.-C. Chang, S.-Y. Wang, S.-C. Chen, C.-C. Lin, S.-C. Chen, P.-W. Chiang, *Appl. Phys. Lett.* **2010**, *96*, 222108.
[34] B. J. Choi, A. B. K. Chen, X. Yang, I. W. Chen, *Adv. Mater.* **2011**, *23*, 3847.
[35] B. K. You, W. I. Park, J. M. Kim, K.-I. Park, H. K. Seo, J. Y. Lee, Y. S. Jung, K. J. Lee, *ACS Nano* **2014**, *8*, 9492.
[36] Q. Liu, S. Long, H. Lv, W. Wang, J. Niu, Z. Huo, J. Chen, M. Liu, *ACS Nano* **2010**, *4*, 6162.
[37] S. Lee, J. Sohn, Z. Jiang, H.-Y. Chen, S.-H. P. Wong, *Nat. Commun.* **2015**, *6*, 8407.
[38] D. Son, J. Lee, S. Qiao, R. Ghaffari, J. Kim, J. E. Lee, C. Song, S. J. Kim, D. J. Lee, S. W. Jun, S. Yang, M. Park, J. Shin, K. Do, M. Lee, K. Kang, C. S. Hwang, N. Lu, T. Hyeon, D.-H. Kim, *Nat. Nanotechnol.* **2014**, *9*, 397.
[39] S. Ban, O. Kim, *Jpn. J. Appl. Phys.* **2014**, *53*, 06JE15.
[40] Z. Fang, H. Yu, W. Liu, Z. Wang, X. Tran, B. Gao, J. Kang, *IEEE Electron Device Lett.* **2010**, *31*, 476.
[41] W. He, K. Huang, N. Ning, K. Ramanathan, G. Li, Y. Jiang, J. Sze, L. Shi, R. Zhao, J. Pei, *Sci. Rep.* **2014**, *4*, 4755.
[42] Y. Li, Y. Zhong, J. Zhang, L. Xu, Q. Wang, H. Sun, H. Tong, X. Cheng, X. Miao, *Sci. Rep.* **2014**, *4*, 4906.
[43] B. Gao, Y. Bi, H.-Y. Chen, R. Liu, P. Huang, B. Chen, L. Liu, X. Liu, S. Yu, H. S. P. Wong, J. Kang, *ACS Nano* **2014**, *8*, 6998.
[44] P. Cappelletti, A. Modelli, *Flash Memories*, Springer, Boston, MA **1999**, p. 399.
[45] S. Larentis, F. Nardi, S. Balatti, D. C. Gilmer, D. Ielmini, *IEEE Trans. Electron Dev.* **2012**, *59*, 2468.
[46] F. Nardi, S. Larentis, S. Balatti, D. C. Gilmer, D. Ielmini, *IEEE Trans. Electron Devices* **2012**, *59*, 2461.
[47] P. R. Mickel, A. J. Lohn, C. D. James, M. J. Marinella, *Adv. Mater.* **2014**, *26*, 4486.
[48] R. Waser, R. Dittmann, G. Staikov, K. Szot, *Adv. Mater.* **2009**, *21*, 2632.
[49] J. Kwon, A. A. Sharma, C.-Y. Chen, A. Fantini, M. Jurczak, A. A. Herzing, J. A. Bain, Y. N. Picard, M. Skowronski, *ACS Appl. Mater. Interfaces* **2016**, *8*, 20176.
[50] K.-C. Chang, T.-C. Chang, T.-M. Tsai, R. Zhang, Y.-C. Hung, Y.-E. Syu, Y.-F. Chang, M.-C. Chen, T.-J. Chu, H.-L. Chen, C.-H. Pan, C.-C. Shih, J.-C. Zheng, S. M. Sze, *Nanoscale Res. Lett.* **2015**, *10*, 1.

Received: October 13, 2016
Revised: January 30, 2017
Published online: March 15, 2017

